



2 Transient creep, aseismic damage and slow failure in Carrara marble 3 deformed across the brittle-ductile transition

4 A. Schubnel,¹ E. Walker,² B. D. Thompson,¹ J. Fortin,³ Y. Guéguen,³ and R. P. Young¹

5 Received 18 April 2006; revised 24 June 2006; accepted 12 July 2006; published XX Month 2006.

7 [1] Two triaxial compression experiments were performed
8 on Carrara marble at high confining pressure, in creep
9 conditions across the brittle-ductile transition. During
10 cataclastic deformation, elastic wave velocity decrease
11 demonstrated damage accumulation (microcracks).
12 Keeping differential stress constant and reducing normal
13 stress induced transient creep events (i.e., fast accelerations
14 in strain) due to the sudden increase of microcrack growth.
15 Tertiary creep and brittle failure followed as damage came
16 close to criticality. Coalescence and rupture propagation
17 were slow (60–200 seconds with ~ 150 MPa stress drops
18 and millimetric slips) and radiated little energy in the
19 experimental frequency range (0.1–1 MHz).
20 Microstructural analysis pointed out strong interactions
21 between intra-crystalline plastic deformation (twinning and
22 dislocation glide) and brittle deformation (microcracking) at
23 the macroscopic level. Our observations highlight the
24 dependence of acoustic efficiency on the material's
25 rheology, at least in the ultrasonic frequency range, and
26 the role played by pore fluid diffusion as an incubation
27 process for delayed failure triggering. **Citation:** Schubnel,
28 A., E. Walker, B. D. Thompson, J. Fortin, Y. Guéguen, and R. P.
29 Young (2006), Transient creep, aseismic damage and slow failure
30 in Carrara marble deformed across the brittle-ductile transition,
31 *Geophys. Res. Lett.*, 33, LXXXXX, doi:10.1029/2006GL026619.

33 1. Introduction

34 [2] Interest in the brittle-ductile transition has increased
35 considerably in recent years, in large part due to the fact that
36 the maximum depth of seismicity corresponds to a transition
37 in the crust and in the upper mantle from seismogenic brittle
38 failure to aseismic cataclastic flow, that is, from localized to
39 homogeneous deformation. The mechanics of the transition
40 depends both on extrinsic variable (state of solid stress, pore
41 pressure, temperature, fluid chemistry and strain rate) and
42 intrinsic parameters (modal composition of the rock, porosity,
43 crack and dislocation density) [Paterson and Wong,
44 2005]. The deformation mechanisms operative during the
45 transition occur on scales ranging from microscopic to
46 macroscopic and have profound influence on the spatiotemporal
47 evolution of stress and deformation [Du *et al.*, 2003],
48 as well as in the coupling of crustal deformation and fluid
49 transport [Miller, 2002]. Thus, investigating the interplay
50 between intragranular plasticity and cracking in the labora-
51 tory may be critical in order to understand the mechanics of

the lower seismogenic zone and/or the early stages of 52
earthquake nucleation [Rice and Cocco, 2006]. 53

[3] In the laboratory, marbles have been studied widely 54
for they can undergo a brittle-plastic transition at room 55
temperature as calcite requires low shear stresses to initiate 56
plastic processes: r -, f -dislocation glide and twinning are 57
activated even at room temperature [Turner *et al.*, 1954]. A 58
number of these studies have documented the mechanical 59
behavior of Carrara marble [Rutter, 1974; Fredrich *et al.*, 60
1989; Renner *et al.*, 2002; Schubnel *et al.*, 2005]. In the 61
cataclastic flow regime, it was demonstrated that deforma- 62
tion is dominated by dislocation creep [Renner *et al.*, 2002], 63
twinning and cracking [Fredrich *et al.*, 1989]. Schubnel *et al.* 64
[2005] showed that the interactions between plastic 65
deformation and brittle processes induced the pore space 66
to either dilate (in creep) or compact (in pure relaxation), 67
without any strain localization taking place. In the present 68
study, two triaxial experiments were performed at room 69
temperature, across the brittle-ductile transition, until failure 70
was finally triggered, in wet and dry conditions respectively. 71

72 2. Experimental Set-Up and Procedure

[4] Two cylindrical samples of Carrara marble (length = 73
80mm, diameter = 40mm) were deformed in a triaxial cell 74
installed at Ecole Normale Supérieure [Schubnel *et al.*, 75
2005]. 2:1 ratio samples were used because of space 76
limitation inside the pressure vessel. This cell is equipped 77
to record strain, permeability, elastic wave velocities and 78
acoustic activity contemporaneously. A network of 14 79
piezoceramic transducers (PZT, eigen frequency 1 MHz) 80
was used in order to measure P wave velocities along 81
several directions. Relative error was 0.5% using cross- 82
correlation and double picking techniques, while the abso- 83
lute error was of the order of a few percents (1–2%). 84
Acoustic Emission (AE) activity was captured using a 85
unique instrument [Thompson *et al.*, 2005, 2006], which 86
stores continuous ultrasonic waveform data onto a 40 GB 87
circular Random Access Memory (RAM) buffer at 10 MHz 88
sampling frequency. The RAM was frozen a few seconds 89
after macroscopic rupture. 90

[5] Inside the vessel, the samples were covered with a 91
neoprene jacket and oil resistant silicon for insulation. 92
Cumulative axial strain was measured using a LVDT 93
located outside the vessel, on top of the piston. Pore 94
pressure was driven by two precision volumetric pumps 95
and water was introduced into the sample through hardened 96
steel end pieces located on the top and bottom of the rock 97
sample. Experiments were performed at room temperature, 98
under wet and dry conditions (termed AeWet and 99
AeDry respectively), using constant stress ramps of 100
 ~ 1 MPa.min P^{-1} . The wet sample was saturated for 101

¹Lassonde Institute, University of Toronto, Toronto, Ontario, Canada.

²Ecole et Observatoire des Sciences de la Terre, Strasbourg, France.

³Laboratoire de Géologie, Ecole Normale Supérieure, Paris, France.

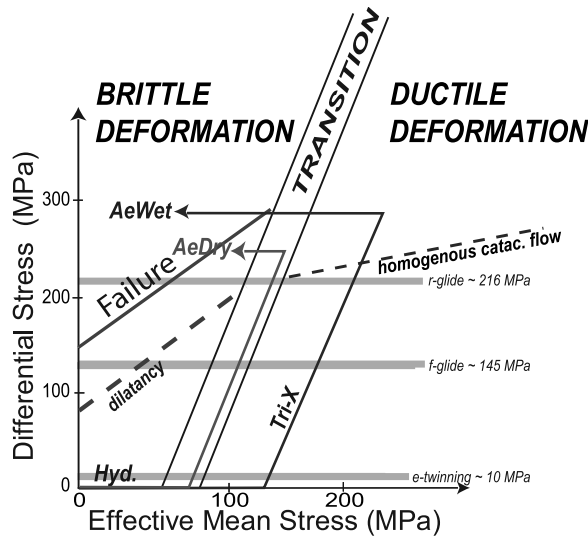


Figure 1. Stress path followed during experiments AeWet and AeDry as a function of differential stress ($\sigma_{B1B} - \sigma_{B3B}$) and effective mean stress $(\sigma_{B1B} + 2\sigma_{B3B})/3 - PB_{pB}$. Onsets of dilatancy^P and homogeneous dilatant cataclastic flow in Carrara marble [from Schubnel et al., 2005], e-twinning, f and r- dislocation in calcite single crystals^P [from Turner et al., 1954] are displayed on the figure.

102 24 hours prior to the experiment and then deformed under
103 drained conditions.

104 [6] A number of studies have already documented the
105 mechanical behavior of Carrara marble along regular tri-
106 axial path [Rutter, 1974; Fredrich et al., 1989; Renner et al.,

2002; Schubnel et al., 2005]. These studies showed that 107
below 50 MPa confinement, deformation is brittle. At 108
higher confinement, cataclastic flow takes place, accompa- 109
nied by strain hardening [Fredrich et al., 1989], damage is 110
homogenous and strain localization does not take place, 111
even at very large strains [Schubnel et al., 2005]. For such 112
reasons, particular stress paths across the brittle-ductile 113
transition were chosen for this study (Figure 1). For AeWet, 114
confining pressure P_c and pore pressure P_p were initially set 115
to 125 MPa and 5 MPa respectively. After irreversible 116
plastic hardening ($\sim 5\%$ plastic axial strain) in the cataclas- 117
tic flow regime, the sample was brought back at constant 118
differential stress ($\sigma_1 - \sigma_3 = 290$ MPa) into the brittle field 119
by increasing pore pressure (P_p) so that the remaining 120
effective confinement ($P_{B_{eff}} = P_c - P_p$) was equal to 121
5MPa. Because no AE activity was observed during this 122
first experiment performed in the wet regime, a second 123
experiment, AeDry, was performed at lower confining 124
pressure, in dry conditions: AeDry sample was initially 125
subjected to 75 MPa confining pressure and 250 MPa 126
differential stress. The confining pressure was then slightly 127
decreased. 128

3. Experimental Results

[7] Figure 2a plots the evolution of differential stress, 130
effective confining pressure, axial strain and P wave veloci- 131
ty with time during AeWet. The onset of plastic deforma- 132
tion was reached at a differential stress value of ~ 150 MPa. 133
From this point, elastic wave velocities decreased rapidly 134
which reveals important damage accumulation. On the 135
contrary, P wave anisotropy increased, which indicates 136
crack propagated along preferential orientations (sub-axial). 137

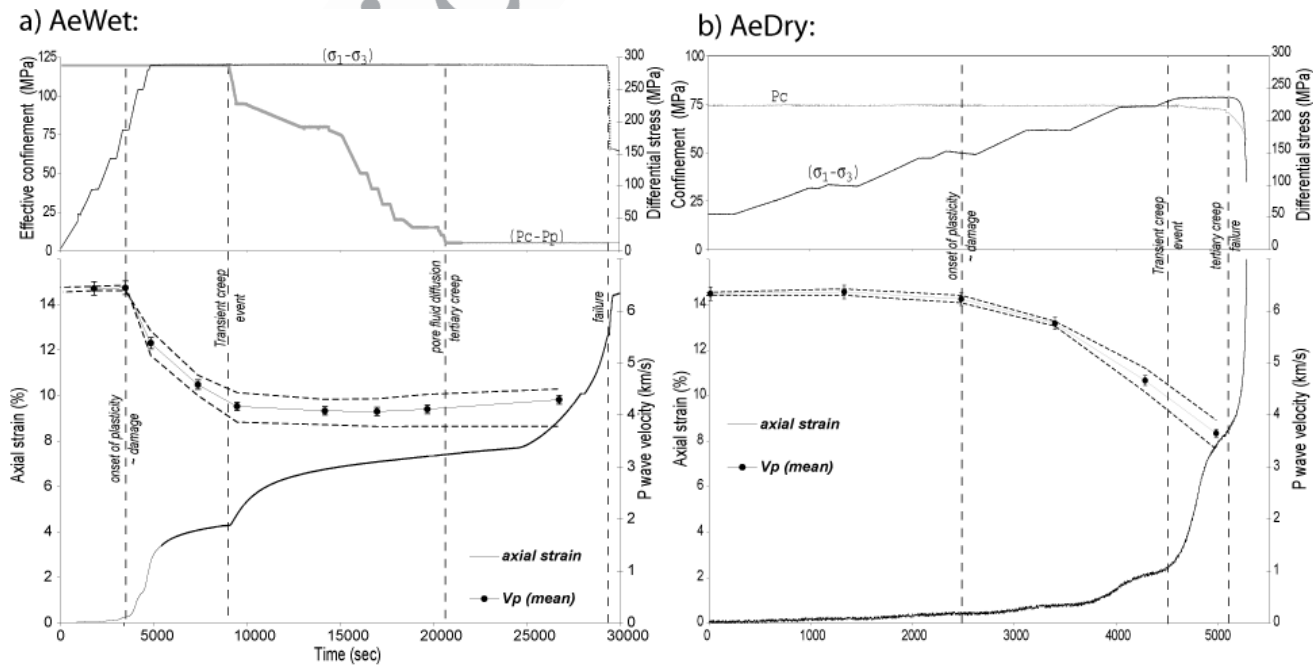


Figure 2. Evolution of differential stress, effective confining pressure, axial strain and P wave velocities vs. time in experiments (a) AeWet and (b) AeDry. Variations in the stress conditions are indicated on the top of the figure ($\sigma_1 - \sigma_3 =$ differential stress, $P_c =$ confining pressure, $P_{cB} - P_{pB} =$ effective confining pressure). Symbols correspond to the mean value of P wave velocities, whereas dashed lines highlight the anisotropy (vertical P wave is fast, horizontal P wave is slow). Transient creep events, onsets of plastic deformation, tertiary creep and failure are indicated.

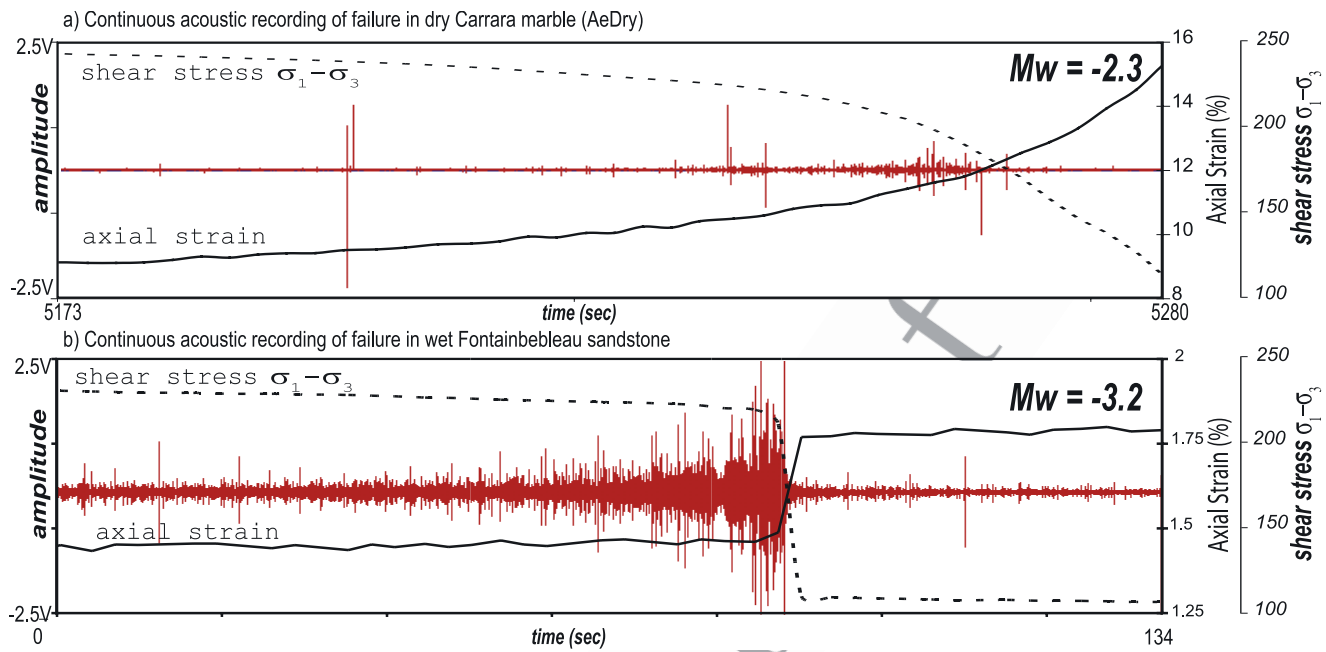


Figure 3. Stress, strain and radiated acoustic energy (frequency range = 0.1–1 MHz). (a) In AeDry: evolution of axial strain, shear stress and acoustic activity (107 seconds segment of the continuous waveform recorded at failure) versus time. (b) In an intact Fontainebleau sandstone (134 seconds continuous waveform recorded at failure). Stress scale is the same in Figures 3a and 3b, not strain scale. Moment magnitudes MB_{WB} , calculated from the mechanical data, are indicated for comparison.

138 As the effective confining stress was lowered at constant
 139 differential stress ($\sigma_1 - \sigma_3 = 290$ MPa), a fast acceleration
 140 in axial strain was observed. This is thought to be due to a
 141 rapid increase in the growth of the existing microcracks,
 142 which were destabilized as normal stress was suddenly
 143 lowered. A few hours after the effective confining pressure
 144 reached its minimal value of 5 MPa, the sample eventually
 145 entered tertiary creep. After 12% cumulative axial shorten-
 146 ing and one hour after the sample entered tertiary creep,
 147 brittle failure finally occurred. The 150 MPa stress drop was
 148 released over approximately 200 seconds. Unlike in purely
 149 brittle materials, no acoustic emission activity was associ-
 150 ated to damage and brittle failure.

151 [8] At lower confinement (75 MPa) and in dry conditions
 152 (Figure 2b), the onset of plasticity was reached at ~ 175 MPa
 153 differential stress. From this point, P wave velocities de-
 154 creased by over 50%, indicating a rapid accumulation of
 155 damage. A rapid increase in anisotropy was also observed
 156 beyond the onset of plasticity, reaching 15% prior to brittle
 157 failure, which remains low when compared to that observed
 158 on dry granite samples deformed in the brittle field
 159 [Stanchits *et al.*, 2003; Schubnel *et al.*, 2003]. A small
 160 decrease (5 MPa) of confinement was sufficient to almost
 161 instantaneously trigger a large transient creep event, fol-
 162 lowed by brittle rupture. This time, time delay to failure was
 163 much shorter (of the order of a few minutes) and again,
 164 damage accumulation and failure initiation triggered no
 165 acoustic emissions. The stress drop was released in approx-
 166 imately 60 seconds.

167 [9] The slips were ~ 1.5 mm and 5 mm in the AeWet and
 168 AeDry respectively. Considering a 60 P^{OP} dipping fault, this
 169 yields seismic moments MB_{OB} (calculated as $MB_{OB} = \mu Au$,

with shear modulus, $\mu = 20$ GPa, fault area $A = 29$ cmP^{2P} 170
 and u as the measured slip) equal to $\sim 1 \times 10P^{5P}$ and $3 \times$ 171
 $10P^5$ PNm , which corresponds to moment magnitudes 172
 (MB_{WB} , calculated using $MB_{WB} = 2/3 \log_{10} BMB_{OB} -$ 173
 6.0) of approximately -2.3 and -2.6 respectively. The 174
 continuous acoustic waveform recorded at rupture in AeDry 175
 (Figure 3a) shows that the peak differential stress cannot be 176
 correlated to any particular acoustic emissions. Brittle 177
 failure therefore seems to have initiated aseismically (at 178
 least in the ultrasonic experimental frequency range, i.e., 179
 0.1–1 MHz). One should note however that, as the slip 180
 accelerated during the latter phase of rupture propagation 181
 and/or frictional sliding, the amount of recorded acoustic 182
 activity increased, which might be due to the shearing of 183
 asperities. In any case, rupture radiated very little energy 184
 compared to what is typically observed on intact silicastic 185
 rocks such as granites [Thompson *et al.*, 2006]. 186

4. Discussion 187

[10] For comparison, Figure 3b displays an example of 188
 the acoustic activity recorded at failure in an intact Fontaine- 189
 bleau sandstone deformed in similar conditions. The 190
 recorded energy is one and a half orders of magnitude 191
 larger than for the AeDry sample, although the calculated 192
 moment magnitude is equal to -3.2 (equivalent to a 200 μm 193
 slip), that is, almost one order of magnitude lower. Attenu- 194
 ation and scattering, larger in the sandstone, cannot be 195
 responsible of the major differences in the two recordings. 196
 However, these differences can be qualitatively understood 197
 when considering that: 1) the fracture toughness of quartz 198
 (~ 1 $MPa \cdot mP^{1/2P}$) is one order of magnitude larger than that 199
 of calcite (~ 0.2 $MPa \cdot mP^{1/2P}$) [Atkinson and Avdis, 1980]; 200

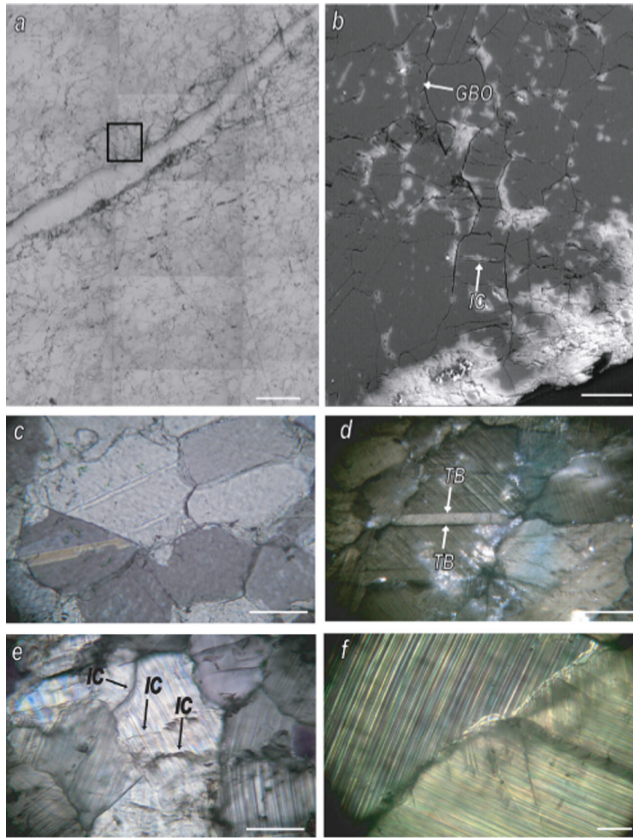


Figure 4. Microstructural analysis. Sections were taken in the horizontal plane, perpendicular to the compression axis. (a) Mosaic image of fractured AeWet sample in reflected light. (b) A SEM image of the fracture wall and its vicinity; the box indicates the location of Figure 1b. (c) Cross-polarized image of an undeformed sample. (d–f) Cross-polarized images of the deformed sample, AeWet, far from the rupture plane. The white scale corresponds to 1mm in Figure 4a; 100 μm in Figure 4b–4e; 20 μm in Figure 4f. IC = intragranular cracks, GBO = grain boundary opening, TB = thick twin boundary.

201 2) in the case of a purely brittle material such as Fontaine-
 202 bleau sandstone, the stress drop is released instantaneously
 203 (<1 second) and the maximum radiated acoustic energy
 204 clearly correlates to the peak stress. This last observation
 205 clearly highlights the dependence of acoustic (and seismic?)
 206 efficiency not only on the rupture propagation speed and the
 207 slip velocity but also on the rock's rheology.

208 [11] Figure 4 presents a series of micrographs of the
 209 fracture plane, which was oriented at ~ 45 degrees from
 210 the vertical. Thin sections were made in a plane perpendic-
 211 ular to the compression axis, in order to show the extent of
 212 the process zone around the main fracture. Figure 4a is a
 213 mosaic in reflected light of the fractured sample AeWet. The
 214 failure plane is narrow (two to three grain diameters wide),
 215 not so rough and filled with very fine gouge material. Only
 216 few intergranular fractures can be observed near the fracture
 217 plane (Figure 4b) and the process zone is narrow
 218 ($\sim < 100 \mu\text{m}$). Figure 4c shows micrographs of an intact
 219 (un-damaged) sample of Carrara marble, while Figures 4d,

4e and 4f show the deformed AeWet sample, in cross- 220
 polarized light. In the intact marble (Figure 4c), few twins 221
 are present initially and grain boundaries are sealed. In the 222
 deformed sample, most of the shear deformation was 223
 accommodated by the presence of mechanical twins at very 224
 high density (Figures 4d, 4e and 4f). Strong interactions 225
 between microcracking and twinning can be observed, as 226
 the bending of twins can nucleate intragranular cracks 227
 (Figure 4e) or induce grain boundary opening (Figures 4b 228
 and 4d). In our experiments, twinning is pervasive at very 229
 high density in all grains (Figure 4f). We observe a 230
 preferential crack nucleation at grain boundaries and twin 231
 intersections which suggest that microcracking could be 232
 caused by dislocation pile-ups (Figure 4d). 233

[12] In calcite bearing rocks and at low temperature, 234
 competition between two basic micromechanisms (mode I 235
 cracking and dislocation glide), controls the macroscopic 236
 behavior (brittle versus ductile). Twinning and dislocation 237
 glide are intra-crystalline processes not sensitive to pressure, 238
 whereas mode I cracking is pressure-sensitive. Twinning is 239
 particularly important when only a limited number of slip 240
 systems are activated in a crystal, as it can palliate the need 241
 of five independent glide systems required for plastic 242
 deformation to take place in any direction [Paterson and 243
 Wong, 2004]. But twin boundaries are obstacles to disloca- 244
 tion glide and randomly oriented grains can only twin along 245
 certain preferential crystallographic directions. This gives 246
 rise to elastic strain incompatibilities and microcracks are 247
 needed in order to accommodate plastic deformation. Both 248
 for AeWet and AeDry, the evolution of crack density was 249
 calculated from P wave velocities evolution (Figure 2) using 250
 two well-established Effective Medium theories: the Non- 251
 Interacting Cracks [Kachanov, 1994] and the Extended 252
 Differential Self-Consistent (DEM) [Le Ravalec and 253
 Guéguen, 1996] methods. The DEM has been proven to be 254
 the most reliable method to calculate the effective elastic 255
 properties of cracked rocks [Orlowsky *et al.*, 2003] as it 256
 takes into account the existing stress interactions between 257
 cracks. However, the non-interacting crack theory, which 258
 neglects stress interactions, is particularly relevant here as 259
 intragranular plasticity tends to inhibit long range stress 260
 interactions. Using matrix Young's modulus and Poisson's 261
 ratio as that of pure calcite, that is, 100 GPa and 0.32 262
 respectively, a fluid bulk modulus equal to that of water, 263
 that is, 2 GPa, P-wave velocities were inverted directly into 264
 crack density using a simple least square fit (see Schubnel *et al.* 265
 [2003, 2006] for details of the inversion method). 266
 Figure 5 illustrates that both inversions (the DEM and the 267
 NIC) give comparable results. Initially, the crack density 268
 decreased from ~ 0.15 to ~ 0.1 as effective mean stress 269
 ($\sigma_{B1B} + 2\sigma_{B3B}$)/3 $- PB_{pB}$ increased, which is synonym of 270
 crack closure. Beyond the onset of plasticity, crack density 271
 increased suddenly due to microcrack nucleation and propa- 272
 gation. At failure, crack density reached values comprised 273
 between 0.7 and 1; 1 being the theoretical percolation 274
 threshold for macroscopic failure in 3 dimensions [Guéguen 275
et al., 1997]. Brittle failure aroused when damage was close 276
 to a critical value, which is consistent with the works of 277
 Baud and Meredith [1997] on Darley Dale sandstone. On 278
 the other hand, the time delay to failure in the wet 279
 experiment is thought to correspond to the time for pore 280
 pressure to diffuse throughout the sample. Such a 281

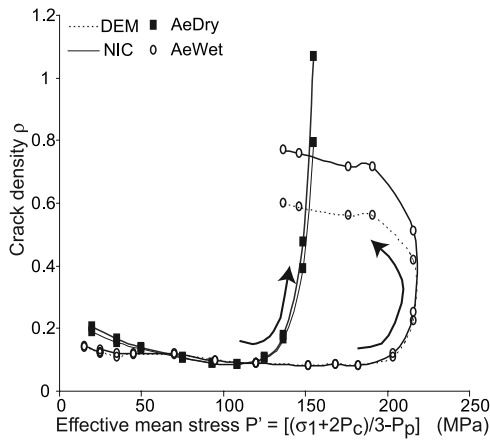


Figure 5. Evolution of the crack density using the Non-Interacting Cracks theory (NIC – solid lines) [Kachanov, 1994] and the Extended Differential Self-Consistent method (DEM – dashed lines) [Le Ravalec and Guéguen, 1996]. Wet (plain symbols) and dry (empty symbols) P-wave velocities (Figures 2a and 2b) were inverted into crack density using both methods (see Schubnel et al. [2003, 2006] for details of the inversion method). Matrix Young's modulus and Poisson's ratio were taken equal 100 GPa and 0.32 respectively, fluid bulk modulus equal to 2 GPa.

282 hypothesis yields a hydraulic diffusivity D of
 283 $\sim 10P^{-8P} \text{ mP}^{2P} \cdot sP^{-1P}$, equivalent to a permeability of $k \sim$
 284 $10P^{-20} \text{ P mP}^{2P}$. This is consistent with our crack density
 285 analysis [Schubnel et al., 2006], the experimental determina-
 286 tion of Carrara marble's permeability at high pressure
 287 [Zhang et al., 1994] and the determination of real fault
 288 gouge permeabilities [Wibberley and Shimamoto, 2003].

289 5. Conclusions and Implications

290 [13] When the confining pressure is sufficient to prevent
 291 mode I cracking, damage in Carrara marble is intra-crystal-
 292 line with twinning and dislocations piling up (as in a cold
 293 worked metal). Because of the low temperatures, dislocation
 294 and twin accumulation is such that cracks are needed in
 295 order to accommodate local plastic differential strain mis-
 296 matches. Lowering the normal stress can induce a short-
 297 lived fast acceleration in strain (i.e., transient creep event),
 298 due to the sudden growth of destabilized microcracks.
 299 However, crack propagation steps radiate small amounts
 300 of energy in the experimental frequency range (0.1–1
 301 MHz), due to the low surface energy of calcite. Radiated
 302 energy might also have been absorbed by neighboring
 303 dislocations [Lawn, 1993] and/or intermittent dislocation
 304 flow [Weiss and Marsan, 2003]. When the crack density
 305 becomes close to a critical value of 1, crack coalescence and
 306 slow brittle failure takes place.

307 [14] Our work clearly highlights the dependence of the
 308 ultrasonic (and seismic?) acoustic efficiency not only on the
 309 rupture propagation speed and the slip velocity but also
 310 the rock's rheology. It also illustrates the possible role
 311 played by pore fluid diffusion as an incubation process
 312 for delayed failure triggering. While in the laboratory, this
 313 could have implications for the mechanics of the lower

seismogenic zone [Du et al., 2003]. There, ductile minerals 314
 prevalent in Earth's crust, such as quartz and feldspar are 315
 predicted to behave in a similar fashion above 300°C as 316
 calcite does at room temperature [Tullis and Yund, 1992]. 317
 Within fault gouges and even at shallower depths, clays 318
 might also behave the same way. 319

[15] **Acknowledgments.** The authors would like to thank P. Benson, 320
 M. H. B. Nasser, D. Collins and the many researchers who, through 321
 numerous discussions, helped to greatly improve this manuscript. This 322
 research was funded via a National Environment Research Council (NERC) 323
 equipment grant, a Natural Sciences and Engineering Research Council of 324
 Canada (NSERC) Discovery Grant and the Fond France Canada pour la 325
 Recherche (FFCR). We would also like to thanks three anonymous 326
 reviewers, who helped to greatly improve this manuscript. 327

References

- Atkinson, B. K., and V. Avdis (1980), Fracture mechanics parameters of 329
 some rock deforming minerals determined using an indentation techni- 330
 que, *Int. J. Rock Mech. Min. Sci., Geomech. Abstr.*, 17, 383–386. 331
 Baud, P., and P. B. Meredith (1997), Damage accumulation during triaxial 332
 creep of Darley Dale sandstone from pore volumetry and acoustic 333
 emission, *Int. J. Rock Mech. Min. Sci.*, 34, 024. 334
 Du, W., L. R. Sykes, B. E. Shaw, and C. H. Scholz (2003), Triggered 335
 aseismic fault slip from nearby earthquakes, static or dynamic effect?, 336
J. Geophys. Res., 108(B2), 2131, doi:10.1029/2002JB002008. 337
 Fredrich, J. T., B. Evans, and T-F. Wong (1989), Micromechanics of the 338
 brittle to plastic transition in Carrara marble, *J. Geophys. Res.*, 94, 4129– 339
 4145. 340
 Guéguen, Y., T. Chelidze, and M. Le Ravalec (1997), Microstructures, 341
 percolation thresholds, and rock physical properties, *Tectonophysics*, 342
 279, 23–35. 343
 Kachanov, M. (1994), Elastic solids with many cracks and related prob- 344
 lems, *Adv. Appl. Mech.*, 30, 259–445. 345
 Lawn, B. R. (1993), *UFracture of Brittle Solids*, Cambridge Univ. Press, 346
 New York. 347
 Le Ravalec, M., and Y. Guéguen (1996), High and low frequency elastic 348
 moduli for a saturated porous/cracked rock—Differential self consistent 349
 and poroelastic theories, *Geophysics*, 61, 1080–1094. 350
 Miller, S. A. (2002), Properties of large ruptures and the dynamical influ- 351
 ence of fluids on earthquakes and faulting, *J. Geophys. Res.*, 107(B9), 352
 2182, doi:10.1029/2000JB000032. 353
 Orlovsky, B., E. H. Saenger, Y. Guéguen, and S. A. Shapiro (2003), Effects 354
 of parallel crack distributions on effective elastic properties—A numer- 355
 ical study, *Int. J. Fract.*, 124, 171–178. 356
 Paterson, M. S., and T-F. Wong (2005), *UExperimental Rock Deformation: 357
 The Brittle Field*, 2Pnd ed., 347 pp., Springer, New York. 358
 Renner, J., B. Evans, and G. Siddiqi (2002), Dislocation creep of calcite, 359
J. Geophys. Res., 107(B12), 2364, doi:10.1029/2001JB001680. 360
 Rice, J. R., and M. Cocco (2006), Seismic fault rheology and earthquake 361
 dynamics, in *The Dynamics of Fault Zones*, edited by M. R. Handy, MIT 362
 Press, Cambridge, Mass. 363
 Rutter, E. H. (1974), The influence of temperature, strain rate and interstitial 364
 water in the deformation of calcite rocks, *Tectonophysics*, 22, 331–334. 365
 Schubnel, A., O. Nishizawa, K. Masuda, X. J. Lei, Z. Xue, and Y. Guéguen 366
 (2003), Velocity measurements and crack density determination during 367
 wet triaxial experiments on Oshima and Toki granites, *Pure Appl. Geo-* 368
phys., 160, 869–887. 369
 Schubnel, A., J. Fortin, L. Burlini, and Y. Guéguen (2005), Damage and 370
 recovery of calcite rocks deformed in the cataclastic regime, in *High* 371
Strain Zones, edited by D. Bruhn and L. Burlini, *J. Geol. Soc. London*, 372
 245, 203–221. 373
 Schubnel, A., P. M. Benson, B. D. Thompson, J. F. Hazzard, and R. P. 374
 Young (2006), Quantifying damage, saturation and anisotropy in cracked 375
 rocks by inverting elastic wave velocities, *Pure Appl. Geophys.*, 163, 376
 947–973. 377
 Stanchits, S. A., D. A. Lockner, and A. V. Ponomarev (2003), Anisotropic 378
 changes in P-wave velocity and attenuation during deformation and fluid 379
 infiltration of granite, *Bull. Seismol. Soc. Am.*, 93, 1803–1822. 380
 Thompson, B. D., R. P. Young, and D. A. Lockner (2005), Observations of 381
 premonitory acoustic emission and slip nucleation during a stick slip 382
 experiment in smooth faulted Westerly granite, *Geophys. Res. Lett.*, 32, 383
 L10304, doi:10.1029/2005GL022750. 384
 Thompson, B. D., R. P. Young, and D. A. Lockner (2006), Observations of 385
 fracture in westerly granite under AE feedback and constant strain rate 386
 loading: Nucleation, quasi-static propagation, and the transition to un- 387
 stable fracture propagation, *Pure Appl. Geophys.*, 163, 995–1019. 388

- 389 Tullis, J., and R. A. Yund (1992), The brittle-ductile transition in feldspar
390 aggregates: And experimental study, in *UFault Mechanics and Transport*
391 *Properties of Rocks*, edited by B. Evans and T.-F. Wong, pp. 89–117,
392 Elsevier, New York.
- 393 Turner, F. J., D. T. Griggs, and H. C. Heard (1954), Experimental deformation
394 of calcite crystals, *Geol. Soc. Am. Bull.*, 65, 883–934.
- 395 Weiss, J., and D. Marsan (2003), Three-dimensional mapping of dislocation
396 avalanches: Clustering and space/time coupling, *Science*, 299, 89–92.
- 397 Wibberley, C. A. J., and T. Shimamoto (2003), Internal structure and per-
398 meability of major strike-slip fault zones: The median tectonic line in Mie
399 Prefecture, southwest Japan, *J. Struct. Geol.*, 25, 59–78.
- Zhang, S., S. F. Cox, and M. S. Paterson (1994), The influence of room 400
temperature deformation on porosity and permeability in calcite aggre- 401
gates, *J. Geophys. Res.*, 99, 15,761–15,778. 402
-
- J. Fortin and Y. Guéguen, Laboratoire de Geologie, Ecole Normale 404
Supérieure, 24, rue Lhomond, F-75231 Paris, France. 405
- A. Schubnel B. D. Thompson, and R. P. Young, Lassonde Institute, 406
University of Toronto, 170 College Street, Toronto, ON, Canada M5S 3E3. 407
(alexandre.schubnel@utoronto.ca) 408
- E. Walker, Ecole et Observatoire des Sciences de la Terre, 5 rue René 409
Descartes, F-67084 Strasbourg, France. 410

Article in Proof